

https://doi.org/10.1070/QEL17365

Study of saturated-absorption resonances on the $^3P_{0,1,2}-{}^3D_{1,2,3}$ transitions of magnesium atoms in a hollow-cathode discharge cell

A.N. Goncharov, O.A. Klimacheva, A.O. Mel'nikova

Abstract. **The saturated-absorption resonances on the $^3P_{0,1,2}-{}^3D_{1,2,3}$ transitions of magnesium atoms in a hollow-cathode discharge cell are studied. The line width (FWHM) for the observed saturated-absorption resonance on the $3^3P_0 \rightarrow 3^3D_1$ transition turns out to be ~220 MHz. Experiments are performed using a system based on a 766-nm diode laser with amplification and frequency doubling in a nonlinear BiBO crystal. The results obtained are of interest for sub-Doppler cooling on the $3^3P_2 \rightarrow 3^3D_3$ transition.**

Keywords: *laser cooling, magnesium, frequency standards, saturated-absorption spectroscopy.*

1. Introduction

Precise time and frequency measurements play an important role in both applied and fundamental research. Frequency standards are most precise among all existing ones. Currently, most attention is paid to the development of frequency standards in the optical range based on laser-cooled and trapped neutral atoms [1] or single ions [2]. The relative frequency uncertainty of the best optical frequency standards reach $\sim 10^{-17}-10^{-18}$. Frequency standards are based on alkaline-earth and similar atoms, such as Yb, Ca, Sr, Hg, Tm, and Mg [3, 4]. Magnesium atoms (^{24}Mg) have a number of advantages in comparison with other alkaline-earth elements used in optical frequency standards. In particular, the simpler electron configuration of magnesium atoms, $1s^22s^22p^63s^2$ (term of the ground state $^1S_0$), in contrast to other atoms, allows one to calculate more exactly [5, 6] the frequency shifts for a clock transition at various physical and technical factors. The frequency shift of the $3^1S_0 \rightarrow 3^3P_j$ transitions ($j = 0, 1$) in Mg due to blackbody radiation is very small [6]. There is a closed resonance transition $3^1S_0 \rightarrow 3^1P_1$ (with a natural linewidth $\gamma = 79$ MHz) in magnesium, which is used for efficient cooling [7]. However, because of the large linewidth, the Doppler temperature limit is fairly high: $T_D = 1.9$ mK. Further sub-Doppler cooling of atoms to temperatures of ~10 μK can be performed using the triplet transition $3^3P_2 \rightarrow 3^3D_3$ at a wavelength of 383 nm with a natural width $\gamma = 26$ MHz [8]. Deep sub-Doppler cooling of atoms is necessary to localise them in 'optical lattices'. Localisation in a spatial region with sizes smaller than the radiation wavelength gives rise to the Lamb–Dicke regime, which completely removes the influence of the linear Doppler effect and recoil effect on the clock transition frequency shift [9]. To implement sub-Doppler cooling of magnesium atoms, one must tune the cooling laser radiation frequency to the cyclic transition $3^3P_2 \rightarrow 3^3D_3$. Below we analyse the possibility of using the saturated-absorption resonance of magnesium atoms in a hollow-cathode discharge absorption cell to this end. Similar studies were performed previously on resonance transitions in calcium [10] and ytterbium [11] atoms, as well as on transitions from metastable levels in strontium atoms [12].

A.N. Goncharov Institute of Laser Physics, Siberian Branch, Russian Academy of Sciences, prosp. Akad. Lavrent'eva 15 B, 630090 Novosibirsk, Russia; Novosibirsk State University, ul. Pirogova 2, 630090 Novosibirsk, Russia; Novosibirsk State Technical University, prosp. Karla Marksa 20, 630092 Novosibirsk, Russia; e-mail: goncharov_an@ngs.ru;
O.A. Klimacheva Institute of Laser Physics, Siberian Branch, Russian Academy of Sciences, prosp. Akad. Lavrent'eva 15 B, 630090 Novosibirsk, Russia; Novosibirsk State Technical University, prosp. Karla Marksa 20, 630092 Novosibirsk, Russia;
A.O. Mel'nikova Novosibirsk State Technical University, prosp. Karla Marksa 20, 630092 Novosibirsk, Russia

Received 11 March 2020; revision received 2 April 2020
Kvantovaya Elektronika **50** (6) 561–565 (2020)
Translated by Yu.P. Sin'kov

2. Experiment

The saturated-absorption resonances were investigated using a laser system with a wavelength $\lambda = 383$ nm, which is based on a diode laser with a working wavelength $\lambda = 766$ nm. The laser components are as follows: a diode emitter Sacher Lasertechnik SAL-780-60, a collimating aspherical lens Thorlabs 352230 ($f = 4.5$ mm, NA = 0.55), and a diffraction grating Thorlabs GR13-1205 (1200 lines mm^{-1}). The external-cavity geometry in the quasi-Littrow configuration is used to implement single-frequency lasing and frequency tuning. The diffraction grating is installed on a piezoelectric actuator (PZT), which makes it possible to tune steplessly the laser frequency in the range of several gigahertz. The laser power is about 60 mW. Some part of this power (~20 mW) is coupled into a laser amplifier based on a diode chip Dilas-TA-0765-1000 (Fig. 1).

The diode laser beam is focused into the amplifier chip by an aspherical lens Thorlabs 352230; the amplified radiation is collimated by the same lens (omitted in Fig. 1). The beam at the amplifier output is highly astigmatic; this astigmatism is compensated for by cylindrical lens (*3*), and the final correction of beam divergence is performed using spherical lens (*4*). The power of 766-nm radiation at the amplifier output is ~1 W.

The laser frequency is stabilised using the transmission peak of an external Fabry–Perot interferometer. Stabilisation is implemented by locking the laser frequency near the interferometer transmission peak using an automatic frequency control system. The interferometer with a base $L = 30$ cm (free spectral range FSR $= c/2L = 500$ MHz) is an

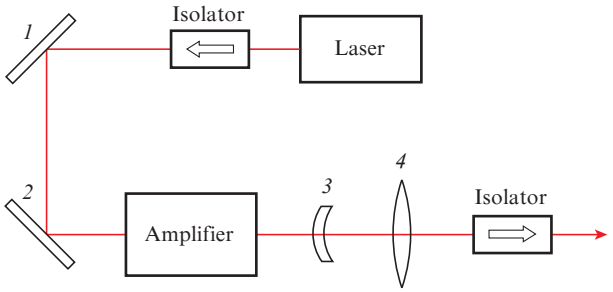

Figure 1. Optical scheme of 766-nm radiation source: (*1*, *2*) plane mirrors; (*3*) cylindrical lens ($f = 15$ cm); (*4*) spherical collecting lens ($f = 75$ cm).

invar rod 80 mm in diameter with an internal hole 10 mm in diameter. Two mirrors are mounted on the rod end faces (the mirror curvature radii and transmittances are, respectively, $R_1 = \infty$, $T = 5\%$ and $R_2 = 50$ cm, $T < 0.1\%$). The mirror with R_2 is installed on a piezoelectric actuator (PZT) for frequency conversion.

The error signal for the frequency stabilisation system was generated by the Pound–Drever–Hall (PDH) locking technique with a modulation frequency of 20 MHz; the laser frequency was modulated using the corresponding modulation of diode laser current. For the feedback loop of the stabilisation system with a bandwidth of ~300 kHz, the radiation linewidth of the laser system at $\lambda = 766$ nm was estimated to be ~100 kHz (estimated by the residual in-loop error signal).

The 383-nm laser radiation was produced as a result of frequency doubling in a nonlinear bismuth triborate (BiBO) crystal placed in an enhancement cavity. The BiBO crystal is most efficient for generating the second harmonic from radiation with $\lambda = 766$ nm, because it has a high optical damage threshold, a wide operating temperature range, and a high optical homogeneity ($\delta n \approx 10^{-6}$ cm^{-1}); in addition, it is not hygroscopic and contains no impurities.

We used a crystal $3 \times 3 \times 10$ mm in size. To increase the second harmonic power, the crystal was placed in an enhancement cavity (Fig. 2).

Using an automatic control system, the cavity length was tuned in resonance with the incident radiation frequency. To this end, an error signal with a frequency of 20 MHz was used in the feedback loop (PDH method). The 383-nm radiation

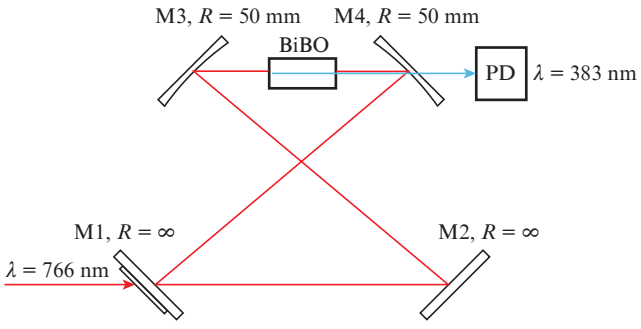

Figure 2. Ring cavity with a BiBO crystal: (M1) plane mirror ($T = 1.2\%$); (M2) plane mirror ($T = 0.03\%$); (M3, M4) spherical dichroic mirrors with a curvature radius $R = 50$ mm.

power exceeded 30 mW. The experimental dependence of the second harmonic power on the input power is presented in Fig. 3.

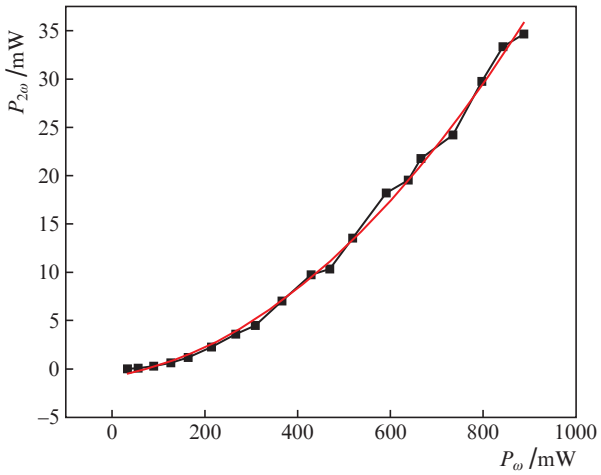

Figure 3. Experimental dependence of the second harmonic power $P_{2\omega}$ on the input power P_ω (the solid line is a second-order polynomial approximation).

Saturated-absorption resonances were observed in a discharge cell with a hollow magnesium cathode L2783-12NE-Mg (Hamamatsu Photonics). In a glow discharge with hollow magnesium cathode, the 3P levels in ^{24}Mg atoms (present in the discharge cell) are populated, due to which the absorption on triplet transitions 3P–3D can be observed. The glow discharge current in our experiment was 15 mA. To detect saturated-absorption resonances, the pump-beam power was modulated (sinusoidal modulation with a depth of 80%) using an acousto-optic modulator (AOM) at a frequency of 20 kHz; the recording signal was detected in the power of a probe weak beam by the lock-in amplifier [10].

A schematic of the system is presented in Fig. 4. It is based on a magnesium hollow-cathode discharge cell filled with neon to a pressure of about 600–700 Pa (the neon pressure in the cell is specified by the manufacturer and may amount to 5–10 Torr). The temperature of magnesium atomic vapour, estimated by us previously from the half-width of Doppler absorption profile $\Delta\nu_D \sim 2$ GHz, is on the order of 1200 K. A plane-parallel plate (PPP) is used to split 383-nm radiation into probe (which does not pass through the AOM) and pump beams. The pump-beam power was modulated by the AOM. To this end, a 180-MHz signal from a generator was amplitude modulated at 20 kHz, transmitted through an amplifier and a power meter (PM), and then applied to the AOM.

The high-frequency (180 MHz) signal power was 1.8 W. The beam diffracted into the AOM first order was used for pumping, due to which the position of the observed saturated-absorption resonances was shifted by half AOM frequency.

The counterpropagating linearly polarised pump and probe beams with a diameter $2w_0 = 3$ mm were aligned in the discharge cell. The powers of these beams were, respectively, $P_{pr} = 0.25$ mW and $P_{pump} = 1.25$ mW.

Saturated-absorption resonances were recorded by laser system frequency tuning and lock-in detection of the signal from photodetector PD2, which registered the probe beam power transmitted through the cell; this approach made

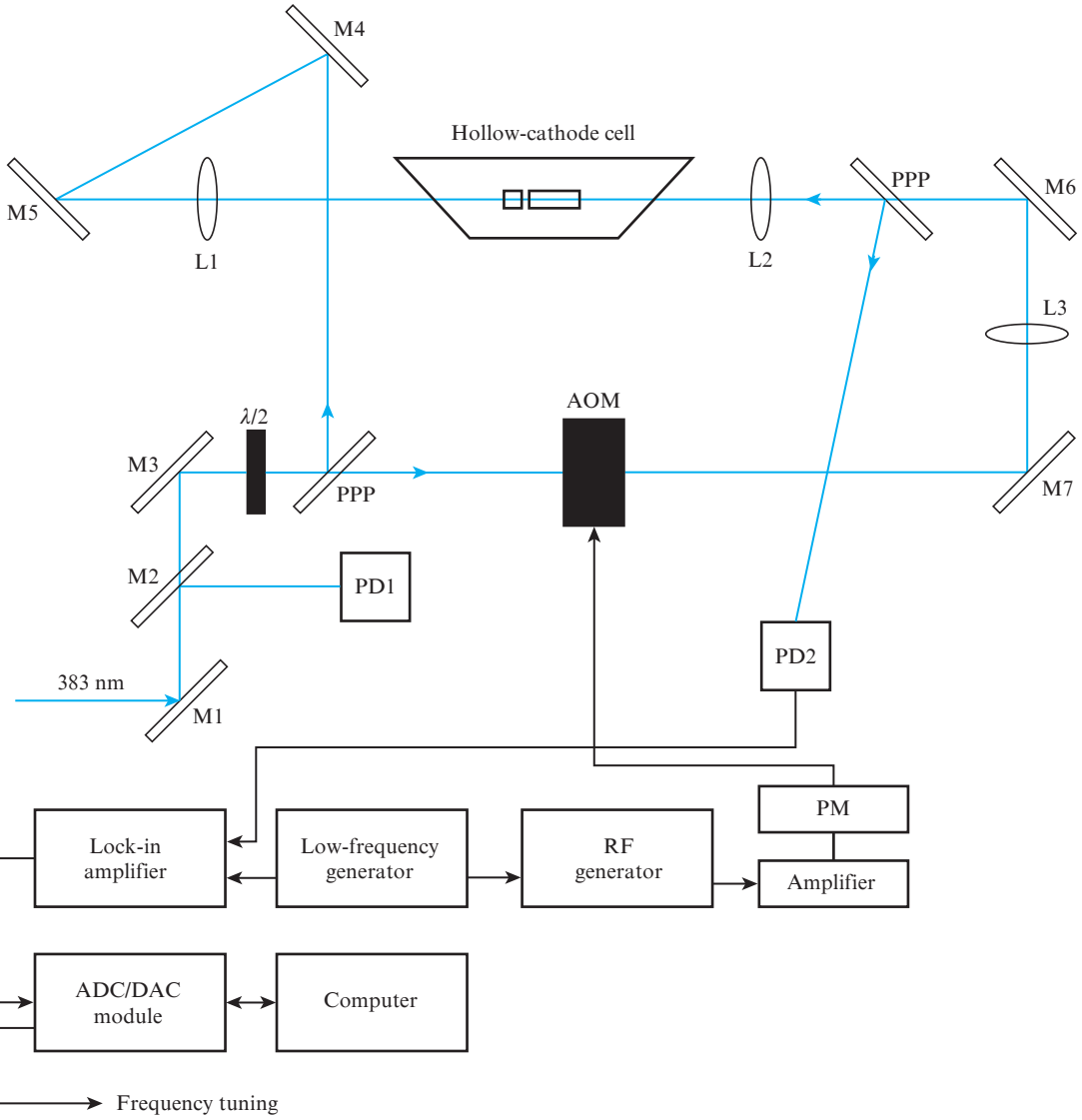

Figure 4. Schematic of the experiment on observing saturated absorption: (M1, M3–M7) high-reflectance mirrors; (M2) mirror with a reflectance of 5%; (L1–L3) collimating lenses; (PPP) uncoated plane-parallel plates; ($\lambda/2$) half-wave phase plate; (AOM) acousto-optic modulator MQ180 (AA Opto-Electronic); (PD1, PD2) photodetectors; (PM) power meter.

it possible to record Lorentz profiles of saturated-absorption resonances.

Note that the observed resonances are planned to be used for tuning radiation frequency to a cooling transition accurate to ~1–10 MHz.

3. Experimental results

To carry out measurements, the diode laser frequency was previously adjusted (with the aid of a wavelength meter) to the desired absorption line of magnesium atoms:

1) $3^3P_0 \to 3^3D_1 - \nu = 782.65772$ THz, $0.5\nu = 391.329$ THz;

2) $3^3P_1 \to 3^3D_2 - \nu = 782.05626$ THz, $0.5\nu = 391.028$ THz;

3) $3^3P_2 \to 3^3D_3 - \nu = 780.8354$ THz, $0.5\nu = 390.417$ THz.

A diagram of the triplet transitions of magnesium atom is shown in Fig. 5.

It can be seen that some transitions have common lower levels. Hence, due to the Doppler broadening, the resonances corresponding to these transitions are overlapped. One should

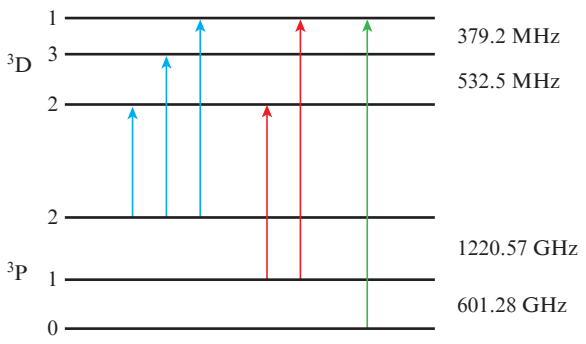

Figure 5. Diagram of levels and triplet transitions in the ^{24}Mg atom [13].

expect additional resonances in the spectrum due to these transitions; they are referred to as cross-resonances. Their intensity is determined as the geometric mean of the intensities of resonances on the transitions between levels [13].

It is convenient to use the isolated transition $3^3P_0 \rightarrow 3^3D_1$ with a relative oscillator strength of 23.8 to study the absorption line shape; the line profile for this transition is presented in Fig. 6.

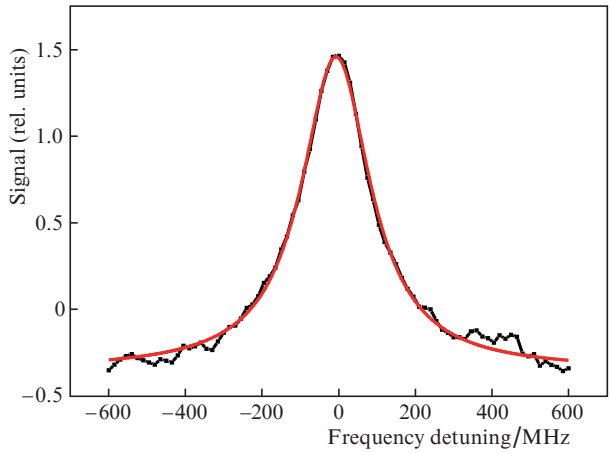

Figure 6. Saturated-absorption resonance on the $3^3P_0 \rightarrow 3^3D_1$ transition (the solid line is an approximation by a Lorenzian with FWHM = 220 MHz). The lock-in amplifier time constant is $\tau = 0.1$ s, the resonance recording time is 30 s, and the number of points is 200.

By analysing the line profile for the $3^3P_0 \rightarrow 3^3D_1$ transition, one can estimate the spectral resolution of the system. The experimentally found linewidth 220 MHz can be determined, for example, by the neon gas pressure (650 Pa) in the cell. The pressure-induced broadening of resonances may exceed 0.15 MHz Pa^{-1}. It can be seen that the resonance shape is close to Lorentzian; this is an indication of weak influence of flight broadening, $\Delta\omega_{fl} = V/D = 150$ kHz, where V is the most probable atomic velocity and D is the beam diameter.

The $3^3P_1 \rightarrow 3^3D_2$ transition has a common lower level with the $3^3P_1 \rightarrow 3^3D_1$ transition; their relative oscillator strengths are, respectively, 53.6 and 17.9. The frequencies of these transitions differ by ~0.91 GHz (see Fig. 5). Peak (1) in Fig. 7 corresponds to the $3^3P_1 \rightarrow 3^3D_2$ transition, and peak (3) corresponds to the $3^3P_1 \rightarrow 3^3D_1$ transition. The spacing between the peaks is 0.93 GHz, which coincides with good accuracy with the distance between the 3^3D_2 and 3^3D_1 levels. Peak (2) is related to the cross signal. All three peaks are equidistant (see Fig. 7).

The $3^3P_2 \rightarrow 3^3D_3$ transition has a common lower level with the $3^3P_2 \rightarrow 3^3D_2$ and $3^3P_2 \rightarrow 3^3D_1$ transitions. However, the $3^3P_2 \rightarrow 3^3D_1$ transition with a relative oscillator strength of 1.2 was not observed in our experiment. Peak (1) (Fig. 8) corresponds to the $3^3P_2 \rightarrow 3^3D_2$ transition with a relative oscillator strength of 17.9, and peak (3) corresponds to the $3^3P_2 \rightarrow 3^3D_3$ transition with a relative oscillator strength of 100. The frequencies of these transitions differ by 0.53 GHz (see Fig. 5.). The experimentally observed frequency difference between the corresponding peaks is 0.51 GHz, which is in good agreement with the data of [14]. Since the cross signal [peak (2)] arises in the middle of the gap between peaks (1) and (3), the peaks are equidistant.

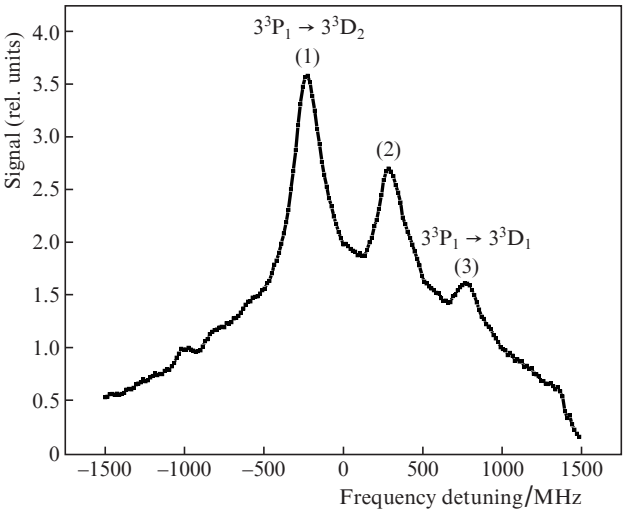

Figure 7. Saturated-absorption resonances on the $3^3P_1 \rightarrow 3^3D_2$ and $3^3P_1 \rightarrow 3^3D_1$ transitions.

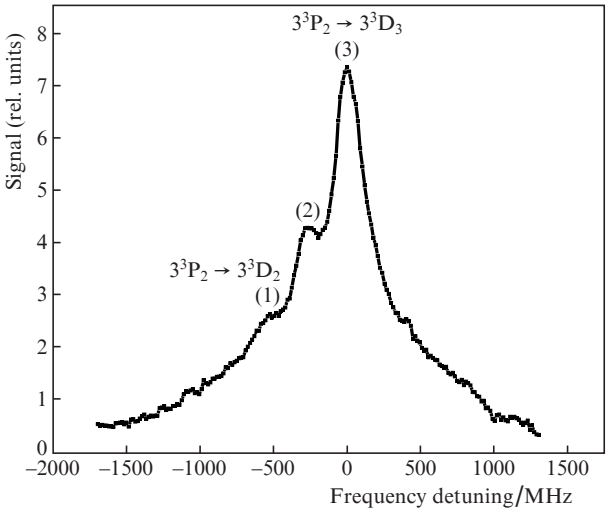

Figure 8. Saturated-absorption resonance on the $3^3P_2 \rightarrow 3^3D_3$ and $3^3P_2 \rightarrow 3^3D_2$ transitions.

Both estimates and experiments showed that the field broadening of the observed resonances is insignificant under our experimental conditions. The saturation intensity for the natural width of cooling transition $3^3P_2 \rightarrow 3^3D$, equal to 26 MHz, is

$$I_{sat} = \frac{2\pi hc\gamma}{3\lambda^3} = 60 \text{ mW cm}^{-2}.$$

For a pump beam with a power of 1 mW and diameter of 3 mm, the laser beam intensity is $I = 15$ mW cm^{-2}, and the saturation parameter is $S_0 = 0.25$.

In this work, we detected for the first time saturated-absorption resonances on triplet transitions 3P–3D with a width of ~200 MHz. The results obtained are planned to be used for frequency tuning in experiments on sub-Doppler cooling of magnesium atoms in a magneto-optical trap.

Acknowledgements. The studies on magnesium spectroscopy were supported by the Russian Foundation for Basic Rese-

arch (Project No. 1902-00514). The work on the laser system frequency stabilisation using the external-cavity transmission band was supported within the State Assignment of the Ministry of Science anf Higher Education of the Russian Federation (Theme No. AAAA-A19119102890006-5).

References

1. Katori H. *Nature Photon.*, **5**, 203 (2011).
2. Rosenband T., Hume D.B., Schmidt P.O., et al. *Science*, **319**, 1808 (2008).
3. Keupp J., Douillet A., Mehlstäubler T.E., Rehbein N., Rasel E.M., Ertmer W. *Eur. Phys. J. D*, **36**, 289 (2005).
4. Goncharov A.N., et al. *Quantum Electron.*, **48** (5), 410 (2018) [*Kvantovaya Elektron.*, **48** (5), 410 (2018)].
5. Friebe J., Riedmann M., Wübbena T., Pape A., Kelkar H., Ertmer W., Terra O., Sterr U., Weyers S., Grosche G., Schnatz H., Rasel E.M. *New J. Phys.*, **13**, 125010 (2011).
6. Kulosa A.P., Fim D., Zipfel K.H., Rühmann S., Sauer S., Jha N., Gibble K., Ertmer W., Rasel E.M., Safronova M.S., Safronova U.I., Porsev S.G. *Phys. Rev. Lett.*, **115**, 240801 (2015).
7. Goncharov A.N., et al. *Quantum Electron.*, **44** (6), 521 (2014) [*Kvantovaya Elektron.*, **44** (6), 521 (2014)].
8. Prudnikov O.N., Brazhnikov D.V., Taichenachev A.V., Yudin V.I., Goncharov A.N. *Quantum Electron.*, **46** (7), 661 (2016) [*Kvantovaya Elektron.*, **46** (7), 661 (2016)].
9. Katori H., Takamoto M., Pal'chikov V.G., Ovsiannikov V.D. *Phys. Rev. Lett.*, **91**, 173005 (2003).
10. Dammalapati U., Norris I., Riis E. *J. Phys. B: At. Mol. Opt. Phys.*, **42**, 165001 (2009).
11. Takehiko T. et al. *Jpn. J. Appl. Phys.*, **57**, 062501 (2018).
12. Hayakawa Y. et al. *Appl. Opt.*, **57** (6), 1450 (2018).
13. Mandal S., Ghosh P.N. *Phys. Rev. A*, **45** (7), 4990 (1992).
14. Beverini N., Cai W.Q., et al. *Opt. Commun.*, **110** (3-4), 309 (1994).